Integral analysis of boundary layer flows with pressure gradient

Tie Wei, Yvan Maciel, and Joseph Klewicki

Phys. Rev. Fluids **2**, 092601 — Published 21 September 2017

DOI: 10.1103/PhysRevFluids.2.092601

Integral Analysis of Boundary Layer Flows with Pressure Gradient

Tie Wei,* Yvan Maciel,† and Joseph Klewicki‡

(Dated: September 11, 2017)

Abstract

This paper investigates boundary layer flows with pressure gradient using a novel similarity/integral analysis of the continuity equation and momentum equation in the streamwise direction. The analysis yields useful analytical relations for V_e, the mean wall-normal velocity at the edge of the boundary layer, and for the skin friction coefficient, C_f, in terms of the boundary layer parameters and in particular β_{RC}, the Rotta-Clauser pressure gradient parameter. The analytical results are compared with experimental and numerical data and are found to be valid. One of the main findings is that for large positive β_{RC} (important effect of an adverse pressure gradient), the friction coefficient is closely related to β_{RC} as $C_f \propto 1/\beta_{RC}$, because δ/δ_1, $\delta_1/\delta_2 = H$ and $d\delta/dx$ become approximately constant. Here δ is the boundary layer thickness, δ_1 is the displacement thickness, δ_2 is the momentum thickness and H is the shape factor. Another finding is that the mean wall-normal velocity at the edge of the boundary layer is related to other flow variables as $U_e V_e/u_\tau^2 = H + (1 + \delta/\delta_1 + H)\beta_{RC}$, where U_e is the streamwise velocity at the edge of the boundary layer. At zero pressure gradient, this relation reduces to $U_\infty V_\infty/u_\tau^2 = H$ as recently derived by Wei and Klewicki[1].

* Department of Mechanical Engineering, New Mexico Institute of Mining and Technology.; tie.wei@nmt.edu

† Department of Mechanical Engineering, Université Laval; Yvan.Maciel@gmc.ulaval.ca

‡ Department of Mechanical Engineering, University of New Hampshire; Department of Mechanical Engineering, University of Melbourne; joe.klewicki@unh.edu; klewicki@unimelb.edu.au

I. INTRODUCTION

Turbulent boundary layer flows subject to pressure gradient occur in many engineering applications, for example diffusers, turbine blades, trailing edges of airfoils and the aft section of ship hulls. In particular, turbulent boundary layer flows with adverse pressure gradient (APG) often play a critical role in determining the performance of engineering devices. Under strong APG the boundary layer flow may separate from the solid surface, causing a drastic change to the flow pattern. In many occasions, accurate knowledge of the adverse pressure gradient boundary layer development is the most critical factor in predicting the overall performance of the device.

Due to its significance, the APG TBL has been the subject of numerous theoretical, experimental and numerical studies over the past six decades. The idea behind the equilibrium turbulent boundary layer was laid out by Rotta [2] and by Clauser [3], who examined a boundary layer with a well defined and simple pressure history. Clauser defined an equilibrium profile as one of a set of profiles in which a constant force history is obtained. In his analysis Clauser introduced a non-dimensional pressure gradient parameter β_{RC}, commonly called Rotta-Clauser parameter:

$$\beta_{RC} = \frac{\delta_1}{u_\tau^2}\frac{1}{\rho}\frac{dP}{dx} = -\frac{\delta_1}{u_\tau^2}U_e\frac{dU_e}{dx}, \tag{1}$$

where δ_1 is the displacement thickness of the boundary layer, $u_\tau = \sqrt{\tau_w/\rho}$ is the friction velocity and U_e is the free stream velocity.

Following Rotta and Clauser, during the last six decades numerous researchers have studied the APG TBL, analytically, experimentally and numerically, e.g., [4–14]. Our knowledge and understanding of boundary layer flows with pressure gradient are, however, still incomplete.

The goal of the present study is to use integral and similarity analysis to gain a better understanding of the relationship between important parameters of PG TBLs. The relationships analytically developed herein are useful for the physical understanding of such flows, and to estimate important flow parameters. Integral analysis of the boundary layer equations is almost as old as boundary layer theory itself (Pohlhausen 1921[15], von Kármán 1921[16]). In the case of turbulent boundary layers, it has led to a panoply of integral methods that continue to be used in engineering analysis. It is important to stress that the present similarity/integral analysis was not, however, performed to design a new integral method to compute turbulent boundary layers or to obtain closure relationships for integral methods. Rather, the novelty of the present integral analysis is twofold. The first relates to the manner in which the integral continuity and momentum equations are combined. The second is that the integral equations are expressed in terms of the pressure gradient parameter. This is convenient and useful because of the importance of this parameter in describing PG flows.

One of the unique objectives of the present study is to investigate how the mean wall-normal velocity at the edge of APG TBLs, V_e, evolves under the action of a pressure gradient. In the traditional integral analysis, the mean wall-normal velocity is not explicitly utilized. In fact, due to its small magnitude, the mean wall-normal velocity has been largely ignored in previous studies of turbulent boundary layer flows. In ZPG boundary layer flows, the mean wall-normal velocity monotonically increases from 0 at the surface to a maximum value outside the boundary layer as sketched in figure 1. However, in boundary layer flows with APG, the mean wall-normal velocity continues to increase outside the boundary layer as also illustrated in figure 1.

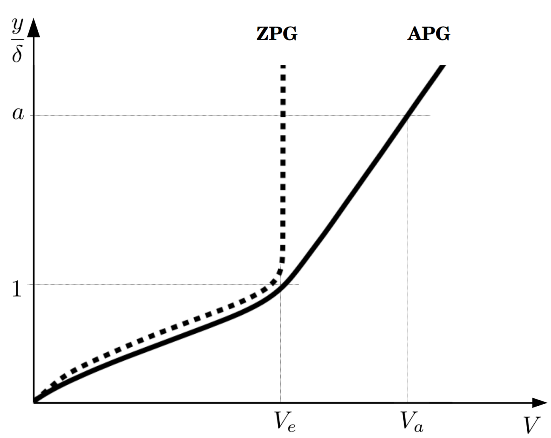

FIG. 1. *Sketch illustrating the shape of the mean wall-normal velocity in boundary layer flows with zero-pressure-gradient (ZPG) or adverse-pressure-gradient (APG).*

We start the analysis by assuming self-similarity of the velocity moments in the continuity equation and the streamwise mean momentum balance equation. Subsequent integration of both equations from the surface at $y = 0$ to outside the boundary at $y = a\delta$ (see Fig. 1) yields relationships for V_e and C_f in terms of the boundary layer parameters, and in particular in terms of β_{RC}. Experimental and numerical data are compared with these analytical relations, and the overall agreement is assessed.

II. SIMILARITY/INTEGRAL ANALYSIS

This work considers two-dimensional boundary layer flows in which the mean flow only varies in the streamwise x and wall-normal y directions, and is statistically homogeneous in the spanwise direction z. The governing equations for the 2D boundary layer flows, i.e., the continuity equation and mean momentum balance equation in the streamwise direction, are

$$\frac{\partial U}{\partial x} + \frac{\partial V}{\partial y} = 0, \tag{2}$$

$$U\frac{\partial U}{\partial x} + V\frac{\partial U}{\partial y} - \nu\frac{\partial^2 U}{\partial y^2} - \frac{\partial T}{\partial y} + \frac{1}{\rho}\frac{dP}{dx} = 0, \tag{3}$$

where $T = -\langle u'v'\rangle$ is the kinematic Reynolds shear stress. (Note that the contribution of $\partial\langle u'u'\rangle/\partial x$ is neglected in the present analysis. Near separation and for strongly accelerated/decelerated flows, such an assumption might not be adequate.) Setting T to zero results in the equation for laminar boundary layer flows. As the Reynolds shear stress is zero at the wall and outside the boundary layer, the present analysis also applies to laminar boundary layers with pressure gradient.

The only assumption in the following development is that the boundary layer is assumed to be self-similar. This is of course not the case for many PG flows since they are often not in dynamic equilibrium. Imposing self-similarity of the velocity moments is equivalent to assuming that the TBL is in a state of quasi-equilibrium. The next section will demonstrate under what conditions this assumption can be considered to approximately hold.

In this work, the boundary layer thickness δ and the streamwise velocity U_e at the edge of the boundary layer are used to normalize the flow variables. The normalized flow variables are

$$U^*(\eta) \equiv \frac{U(x,y)}{U_e(x)}; \quad V^*(x/\delta,\eta) \equiv \frac{V(x,y)}{U_e(x)}; \quad T^*(x/\delta,\eta) \equiv \frac{T(x,y)}{U_e^2(x)}; \quad \eta \equiv \frac{y}{\delta(x)}. \tag{4}$$

Assuming self-similarity for U^* (V^* and T^* do not need to be assumed self-similar as the equations do not involve $\partial V/\partial x$ or $\partial T/\partial x$), the normalized derivatives appearing in the governing equations are as listed in table I. Note that the assumed self-similarity $U^*(\eta)$ does not contradict the classical self-similarity assumption [2, 3]: $(U_e - U)/u_\tau = \hat{U}(\eta)$.

Self-similarity of the TBL requires u_τ/U_e =constant [5, 11]. It follows that $U/u_\tau = f(\eta)$ and hence $U/U_e = U^*(\eta)$. Consequently, the present analysis recasts the continuity and momentum equations in different forms than in the classical similarity analysis, but it does not contradict it in any manner.

$\frac{\partial U}{\partial x} = -\frac{U_e}{\delta}\frac{d\delta}{dx}\eta\frac{\partial U^*}{\partial \eta} + \frac{dU_e}{dx}U^*,$	$\frac{\partial U}{\partial y} = \frac{U_e}{\delta}\frac{\partial U^*}{\partial \eta},$	$\frac{\partial^2 U}{\partial y^2} = \frac{U_e}{\delta^2}\frac{\partial^2 U^*}{\partial \eta^2}.$
$\frac{\partial V}{\partial y} = \frac{U_e}{\delta}\frac{\partial V^*}{\partial \eta},$	$\frac{\partial T}{\partial y} = \frac{U_e^2}{\delta}\frac{\partial T^*}{\partial \eta}.$	

TABLE I. Normalized derivatives in the governing equations.

Substituting the normalized derivatives, the non-dimensional continuity equation becomes

$$\frac{\partial V^*}{\partial \eta} = \frac{d\delta}{dx}\eta\frac{\partial U^*}{\partial \eta} - \frac{\delta}{U_e}\frac{dU_e}{dx}U^*. \tag{5}$$

Integrating this equation from the surface $\eta = 0$ to outside the boundary layer $\eta = a$ (where $a \geq 1$) yields

$$\frac{V_a}{U_e} = \frac{d\delta}{dx}\frac{\delta_1}{\delta} + \frac{u_\tau^2}{U_e^2}\Big(a\frac{\delta}{\delta_1} - 1\Big)\beta_{RC}. \tag{6}$$

Multiplying U_e^2/u_τ^2 on both sides of equation 6 yields

$$\frac{U_e V_a}{u_\tau^2} = \frac{\delta_1}{\delta}\frac{d\delta}{dx}\frac{U_e^2}{u_\tau^2} + \Big(a\frac{\delta}{\delta_1} - 1\Big)\beta_{RC}. \tag{7}$$

In many previous experiments, V is not measured. However, if $d\delta/dx$ can be extracted from measurements, equation 7 can be used to calculate $U_e V_a/u_\tau^2$, indirectly.

Substituting the normalized variables, the non-dimensional mean momentum equation in the streamwise direction becomes

$$-U^*\frac{\partial V^*}{\partial \eta} + V^*\frac{\partial U^*}{\partial \eta} - \frac{\nu}{\delta U_e}\frac{\partial^2 U^*}{\partial \eta^2} - \frac{\partial T^*}{\partial \eta} + \frac{\delta}{\delta_1}\frac{u_\tau^2}{U_e^2}\beta_{RC} = 0. \tag{8}$$

Replacing $\partial V^*/\partial \eta$ from the continuity equation 5, and integrating equation 8 from $\eta = 0$ to $\eta = a$ yields

$$-\frac{d\delta}{dx}\Big(\frac{\delta_1}{\delta} + \frac{\delta_2}{\delta}\Big) - 2\frac{\delta}{\delta_1}\Big(a - \frac{\delta_1}{\delta} - \frac{\delta_2}{\delta}\Big)\frac{u_\tau^2}{U_e^2}\beta_{RC} + \frac{V_a}{U_e} + \frac{u_\tau^2}{U_e^2} + a\frac{\delta}{\delta_1}\frac{u_\tau^2}{U_e^2}\beta_{RC} = 0. \tag{9}$$

Combining equations 6 and 9 yields a relation for V_a

$$\frac{U_e V_a}{u_\tau^2} = H + \Big(1 + a\frac{\delta}{\delta_1} + \frac{\delta_1}{\delta_2}\Big)\beta_{RC}, \tag{10}$$

or

$$U_e V_a = H u_\tau^2 + \Big(1 + a\frac{\delta}{\delta_1} + \frac{\delta_1}{\delta_2}\Big)\delta_1 \frac{1}{\rho}\frac{dP}{dx}. \tag{11}$$

At separation $u_\tau = 0$, and thus

$$U_e V_a = \Big(1 + a\frac{\delta}{\delta_1} + \frac{\delta_1}{\delta_2}\Big)\delta_1 \frac{1}{\rho}\frac{dP}{dx}, \quad \text{or} \quad V_a = -\Big(1 + a\frac{\delta}{\delta_1} + \frac{\delta_1}{\delta_2}\Big)\delta_1 \frac{dU_e}{dx}. \tag{12}$$

Setting $a = 1$ in the above relations produces the scaling for the mean wall-normal velocity at the edge of the boundary layer, V_e.

For zero-pressure gradient boundary layer flows where $\beta_{RC} = 0$, equation 10 recovers the relation derived by Wei and Klewicki[1]

$$\frac{U_\infty V_\infty}{u_\tau^2} = H. \tag{13}$$

Equating the right hand sides of equations 7 and 10 yields

$$C_f = \frac{2\frac{\delta_1}{\delta}\frac{d\delta}{dx}}{H + (2+H)\beta_{RC}}. \tag{14}$$

For $\beta_{RC} >> 1$, the experimental and numerical data below indicate that $\delta_1/\delta \approx 0.5$, $H = \delta_1/\delta_2 \approx 3 - 4$ and $d\delta/dx \approx 0.08 - 0.24$. Thus, at large β_{RC} the friction coefficient can be approximated by

$$C_f \approx \frac{2\frac{\delta_1}{\delta}\frac{d\delta}{dx}}{2+H}\frac{1}{\beta_{RC}} \approx \frac{0.01 \sim 0.03}{\beta_{RC}}. \tag{15}$$

To our knowledge, the above analytical relations are new. Before comparing them with data, a few remarks are warranted. First, it should be noted that C_f and β_{RC} are also linked by virtue of their definitions (see eq. 1):

$$C_f = -\frac{2\delta_1}{U_e}\frac{dU_e}{dx}\frac{1}{\beta_{RC}}. \tag{16}$$

However, in this case the external flow parameters, namely the external velocity and its streamwise derivative, appear explicitly. In contrast, equation 14 solely involves parameters that are directly related to the structure of the boundary layer. Arguably, these parameters better reflect the state of the boundary layer, since the boundary layer does not respond instantly to pressure gradient variations. Consequently, we are able to obtain the approximation at large β_{RC} given by equation 15.

It is also interesting to observe that the approximations that led to equation 15 can be linked to the similarity analyses of turbulent boundary layers as developed by Rotta[2, 5] and Maciel et al.[11]. In the latter analyses, self-similarity implies that

$$\frac{d\delta}{dx} = const, \quad H = const, \quad \frac{\delta_1}{\delta} = const. \tag{17}$$

To our knowledge, equilibrium TBLs represent the only case where these parameters are known to be constant.

Self-similarity also implies

$$\Lambda = -\frac{\delta}{U_e}\left(\frac{d\delta}{dx}\right)^{-1}\frac{dU_e}{dx} = const. \tag{18}$$

Combining equations 16 and 18 yields a relation for C_f similar to equation 15,

$$C_f = \Lambda \frac{2\delta_1}{\delta}\frac{d\delta}{dx}\frac{1}{\beta_{RC}}. \tag{19}$$

Comparison of equations 15 and 19 results in a relation for self-similar TBLs at large β_{RC}

$$\Lambda \approx \frac{1}{2+H} \approx 0.17 \sim 0.25. \tag{20}$$

In equation 20 it is assumed that $2 \leq H \leq 4$. This range of values of Λ indeed corresponds to the values usually found in the case of large-defect self-similar TBLs [11].

Finally, combining equations 14 and 19 yields an exact relation valid for all self-similar TBLs

$$\Lambda = \frac{\beta_{RC}}{H + (2+H)\beta_{RC}}. \tag{21}$$

Note that a relation equivalent to equation 21 has been obtained by Rotta [5], but with $u_\tau/U_e * G$ instead of H, and Δ instead of δ. Skote, Henningson and Henkes [17] presented the relation with δ_1 instead of δ.

III. COMPARISONS WITH NUMERICAL AND EXPERIMENTAL DATA

The analytical relations developed are now compared with experimental and numerical simulation data of APG TBLs. Experiments include those by Angele and Muhammad-Klingmann (AM)[12], Indinger [9], Knopp et al.[18], Maciel et al.[11], Marusic and Perry (MP)[10], Shafiei Mayam[19] and Skare and Krogstad (SK)[20]. In the case of numerical simulations, we use the DNS data of Gungor et al. (GMSS)[21], Skote and Henningson (SH)[22], Spalart and Watmuff (SW)[23], and the LES data of Hickel [13]. All these flows are non-equilibrium TBLs whose mean velocity defect increases in the streamwise direction.

In the case of Skare and Krogstad [20], the last seven streamwise positions out of twelve are in a zone of near equilibrium, with almost self-similar mean velocity and Reynolds stress profiles. Hickel's LES [13] is an attempt to numerically reproduce the flow case of Indinger [9]. These two flows are therefore similar and represent a strongly decelerated situation with massive separation downstream. The other flows constitute different dynamical evolutions of the mean momentum balance.

Since δ/δ_1, H, and $d\delta/dx$ are the parameters in the derived relations for V_e and C_f, we first present experimental and numerical data of these parameters as a function of β_{RC}. Figure 2 shows that, as expected, (1) $\frac{\delta}{\delta_1}$ decreases, monotonically, from a value of about 10 to about 2 at very large β_{RC}, and (2) H increases, monotonically, from a value of about $1.3-1.4$ to about $3.5-4$. An interesting point is that both $\frac{\delta}{\delta_1}$ and H vary slowly with β_{RC} for $\beta_{RC} > 100$. Moreover, their variations lead to $S = 1 + \frac{\delta}{\delta_1} + H \approx 6$ for $\beta_{RC} > 10$. S appears in equation 10 for V_e (setting $a = 1$).

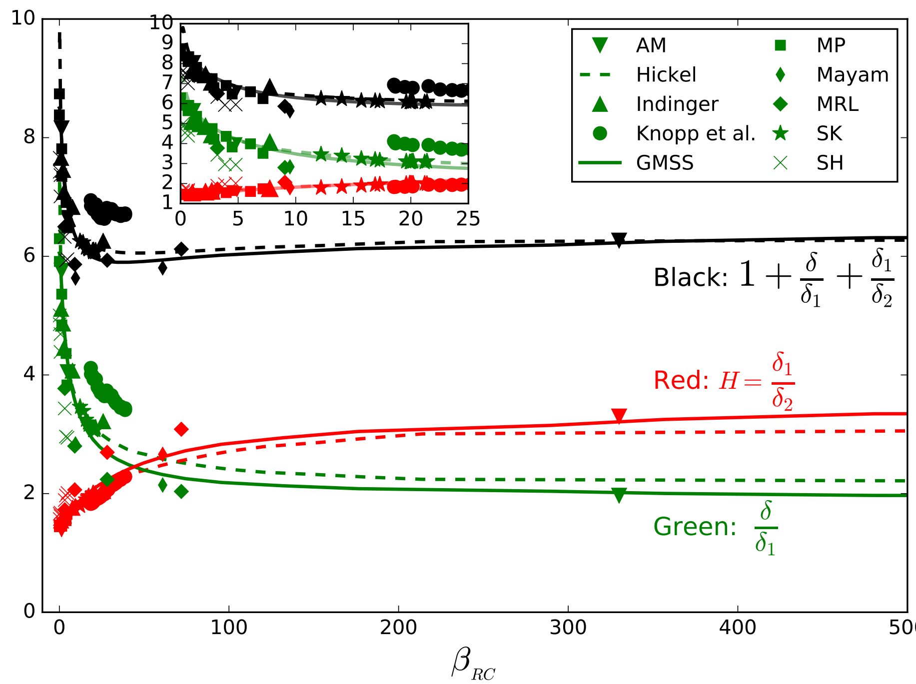

FIG. 2. *Ratio of boundary layer thicknesses. See text for references.*

With the exception of the last seven streamwise positions of SK [20] (the ones with $\beta_{RC} \approx 20$), all the other flows and flow zones are not in equilibrium. Thus, for these cases it is not surprising that $\frac{\delta}{\delta_1}$ and H evolve differently with β_{RC} from one flow to another, as these flows are subject to different upstream history effects[24]. Moreover, the differences between

APG TBLs can be accentuated by Reynolds number effects since the Reynolds number is relatively low for some databases, e.g., the DNS of SH [22] where $Re_\tau \approx 100$. Finally, it is worth pointing out that in most experiments the integral length scales, δ_1 and δ_2, can usually be obtained accurately while the uncertainty of δ is much larger[25].

Figure 3 shows the dependence of the boundary layer growth rate $d\delta/dx$ on β_{RC}. Central finite difference was used to calculate $d\delta/dx$. In many experiments, the distance between $x-$stations is not small, so it is unavoidable that the calculated $d\delta/dx$ has fairly high uncertainty. Nonetheless, it is reasonable to state that at sufficiently large β_{RC}, $d\delta/dx$ varies slowly with β_{RC}. It becomes nearly constant with values in the range $0.08 - 0.24$. More data are, however, needed to verify this. The different values of $d\delta/dx$ for a given β_{RC} are expected since $d\delta/dx$ is strongly dependent on the upstream and local strength of the deceleration/acceleration, as well as the Reynolds number.

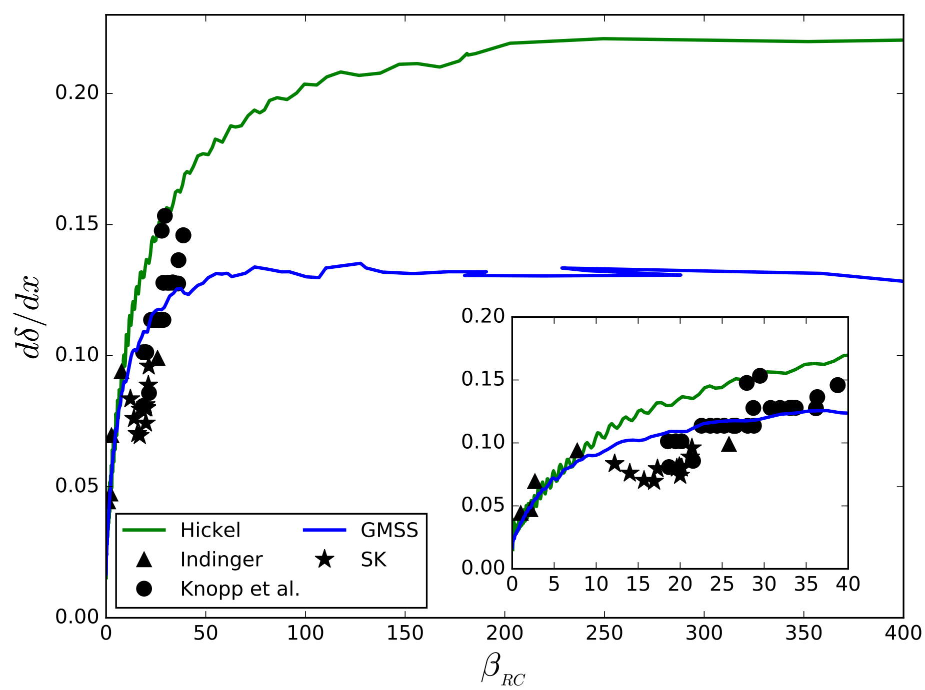

FIG. 3. *Growth rate of boundary layer thickness, $d\delta/dx$, as a function of β_{RC}.*

Figure 4 plots experimentally and numerically determined skin friction coefficient data for varying β_{RC}. The various flows follow different trends of decreasing C_f with β_{RC}. Again, this is expected because of the different streamwise evolutions of these non-equilibrium TBLs, and because of their different Reynolds numbers. Nonetheless, figure 4a shows that the data agree well with the approximate trend predicted by equation 15 for large β_{RC}. It should be

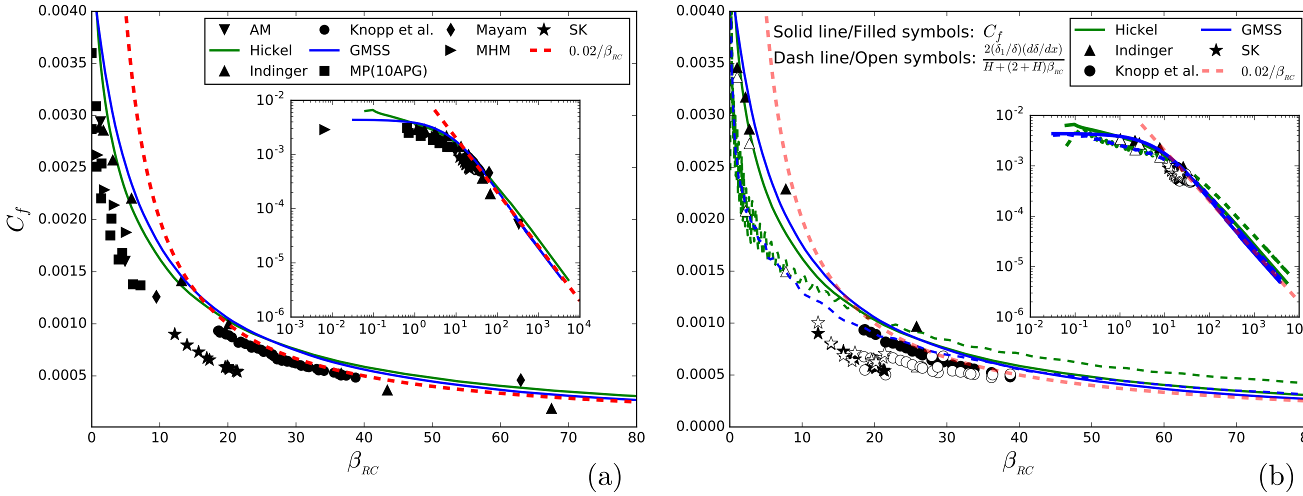

FIG. 4. *(a) Skin friction coefficient in APG TBLs as a function of β_{RC}. (b) Compare analytical relation 14, $C_f = \frac{2\frac{\delta_1}{\delta}\frac{d\delta}{dx}}{H+(2+H)\beta_{RC}}$, with experimental and numerical data.*

noted that experiments with values of β_{RC} larger than 50 are rare. They include AM [12], Indinger [9] and, for the same flow, Maciel et al.[26] and Shafiei Mayam [19]. The DNS of GMSS [21] and the LES of Hickel [13] cover a wider range of β_{RC}, including a region with a separation bubble.

The left and right hand sides of equation 14 are compared in figure 4b for data sets that allow $d\delta/dx$ to be reasonably estimated. Not surprisingly, equation 14, which assumes self-similarity, works essentially perfectly for SK flow (open and filled symbols overlap) since it is in quasi-equilibrium. However, even in the case of the four other flows that are all in strong disequilibrium, both sides of the equation follow similar trends. Equation 14 is therefore seen to be a reasonable approximate relation between C_f and β_{RC} even for non-equilibrium TBLs, at least in the case of a decelerating U_e.

The left and right hand sides of equations 7 and 10 are compared with numerical and experimental data in figure 5. Experimental data of V for APG TBLs are very rare due to the challenges involved in its measurement. Maciel and collaborators have measured V in the case of a strongly decelerated TBL covering a wide range of β_{RC}[19, 26]. In comparison, numerical simulations provide detailed data on all velocity components, including V. However, numerical simulations are in general limited to low to moderate Reynolds numbers.

Figure 5 shows that U_eV_e/u_τ^2 and the right hand sides of equations 7 and 10 grow approximately linearly with β_{RC}, even for the cases having $\beta_{RC} < 10$. Yet, in the latter cases, $\frac{\delta}{\delta_1}$,

H and $d\delta/dx$ vary greatly with β_{RC}. The only exception to this near linear growth occurs for the LES data of Hickel with U_eV_e/u_τ^2 (green line) and the right hand side of equation 7 (dash-dot green line). An explanation has not yet been found for these different behaviors. The smaller differences between U_eV_e/u_τ^2 and the right hand sides of equations 7 and 10 may be due to the difficulties in obtaining accurate estimates of δ and, in the case of experiments, to measurement uncertainties of V_e, u_τ and β_{RC}.

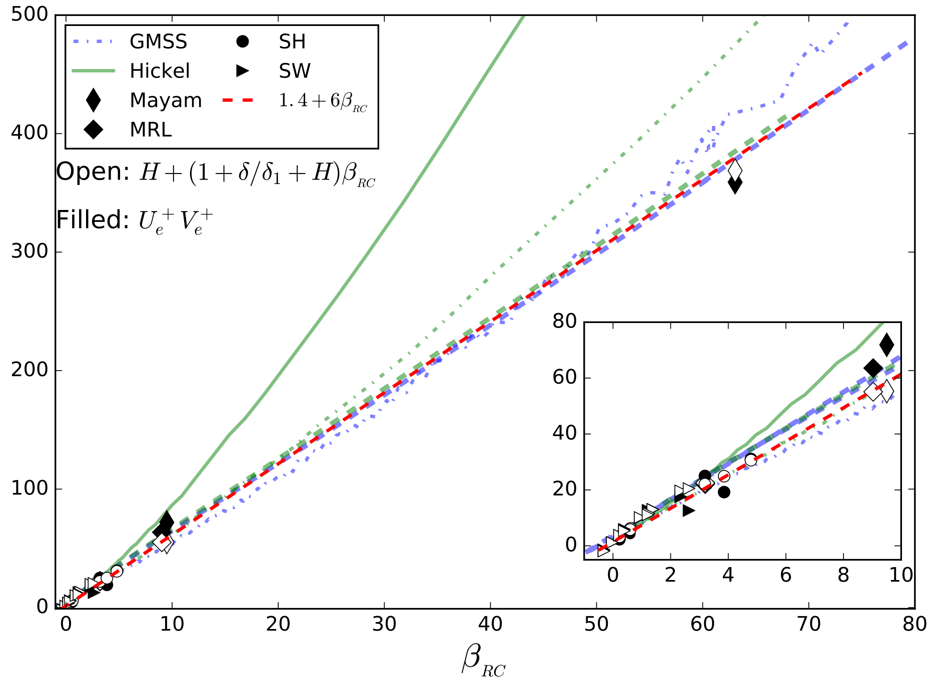

FIG. 5. *Comparing analytical relations 7 and 10 with numerical and experimental data. Filled symbols and solid lines:* U_eV_e/u_τ^2*; Open symbols and dash lines:* $H + (1 + \delta/\delta_1 + H)\beta_{RC}$*. Dash-dot lines: right hand side of equation 7; Red dash line:* $1.4 + 6\beta_{RC}$*. See text for references.*

IV. CONCLUSION

In this work, APG flows are investigated using a new similarity/integral analysis of the continuity and mean momentum equations. Analytical relations are derived for the mean wall-normal velocity at the edge of the boundary layer and for the skin friction coefficient. This approach allows one to determine how these parameters evolve with the Rotta-Clauser pressure gradient parameter. To the authors knowledge, these analytical relations are new. The equation relating skin friction to the Rotta-Clauser pressure gradient parameter is of particular interest. Specifically, the analysis yields an equation that indicates how structural parameters of the boundary layer affect the dependence of skin friction on the Rotta-Clauser pressure gradient parameter. Although the equation is only approximate for non-equilibrium flows, we have shown that the trends are nonetheless well captured by it in the case of decelerating turbulent boundary layers. Furthermore, thanks to this new analytical relation, a simple approximate relation is found between the skin friction coefficient and the Rotta-Clauser parameter for large values of the latter. New relations for self-similar turbulent boundary layers are developed. These explain, for example, the non-dimensional growth rates usually found in experiments at large β_{RC}. Finally, the new relation for the mean wall-normal velocity is of interest since pressure gradients (especially adverse) rather strongly modify boundary layer growth.

Like all other theoretical analyses of PG TBLs, the present analysis assumes local dynamic equilibrium of the flow. Thus, the relations developed cannot account for upstream effects of the pressure gradient, curvature and transition. Not surprisingly, the results presented in this paper suggest that ratios of boundary layer thicknesses, boundary layer growth and skin friction are affected by upstream history effects, at least for moderate values of the pressure gradient parameter. Upstream history effects cannot, however, be isolated from Reynolds number effects with the datasets available in the literature. An important contribution would be to design and conduct future experiments capable of isolating these effects.

V. ACKNOWLEDGMENT

The authors thank Dr. Hickel and Dr. Knopp for generously sharing their data. The financial support of New Mexico Institute of Mining and Technology and Los Alamos National Laboratory (LANL-399931) is gratefully acknowledged by T. W. Y. M. thanks NSERC of Canada for its financial support.

[1] Tie Wei and Joseph Klewicki, “Scaling properties of the mean wall-normal velocity in zero-pressure-gradient boundary layers,” Physical Review Fluids **1**, 082401 (2016).

[2] J. Rotta, “Uber die theorie der turbulenten grenzschichten,” Mitt. Max Planck Inst. Strmungsforsch., Gttingen; translated as On the theory of turbulent boundary layers, NACA Technical

Memorandum No. 1344, 1953 **1** (1950).

[3] F. H. Clauser, "The turbulent boundary layer in adverse pressure gradient," J. Aero. Sci. **21**, 91–108 (1954).

[4] GL Mellor and DM Gibson, "Equilibrium turbulent boundary layers," Journal of Fluid Mechanics **24**, 225–253 (1966).

[5] J.C. Rotta, "Turbulent boundary layers in incompressible flow," Progress in Aerospace Sciences **2**, 1–95 (1962).

[6] Albert A Townsend, *The structure of turbulent shear flow* (Cambridge university press, 1980).

[7] WH Schofield, "Equilibrium boundary layers in moderate to strong adverse pressure gradients," Journal of Fluid Mechanics **113**, 91–122 (1981).

[8] Luciano Castillo and William K George, "Similarity analysis for turbulent boundary layer with pressure gradient: outer flow," AIAA journal **39**, 41–47 (2001).

[9] Thomas Indinger, *Einfluss eines positiven Druckgradienten auf turbulente Grenzschichten an glatten und gerillten Oberflächen*, Ph.D. thesis, Technische Universität München (2005).

[10] Ivan Marušic and AE Perry, "A wall-wake model for the turbulence structure of boundary layers. part 2. further experimental support," Journal of fluid mechanics **298**, 389–407 (1995).

[11] Y. Maciel, K. S Rossignol, and J. Lemay, "Self-similarity in the outer region of adverse-pressure-gradient turbulent boundary layers," AIAA J. **44**, 2450–2464 (2006).

[12] Kristian P Angele and Barbro Muhammad-Klingmann, "PIV measurements in a weakly separating and reattaching turbulent boundary layer," European Journal of Mechanics-B/Fluids **25**, 204–222 (2006).

[13] Stefan Hickel, *Implicit turbulence modeling for large-eddy simulation*, Ph.D. thesis, Universität München (2008).

[14] M Inoue, DI Pullin, Zambri Harun, and I Marusic, "LES of the adverse-pressure gradient turbulent boundary layer," International Journal of Heat and Fluid Flow **44**, 293–300 (2013).

[15] Karl Pohlhausen, "Zur näherungsweisen integration der differentialgleichung der iaminaren grenzschicht," ZAMM-Journal of Applied Mathematics and Mechanics/Zeitschrift für Angewandte Mathematik und Mechanik **1**, 252–290 (1921).

[16] Th. V. von Kármán, "ber laminare und turbulente reibung," ZAMM - Journal of Applied Mathematics and Mechanics / Zeitschrift fr Angewandte Mathematik und Mechanik **1**.

[17] Martin Skote, Dan S Henningson, and Ruud AWM Henkes, "Direct numerical simulation of self-similar turbulent boundary layers in adverse pressure gradients," Flow, turbulence and combustion **60**, 47–85 (1998).

[18] Tobias Knopp, Daniel Schanz, Andreas Schröder, Michnea Dumitra, Christian Cierpka, R Hain, and CJ Kähler, "Experimental investigation of the log-law for an adverse pressure gradient turbulent boundary layer flow at $Re_\theta = 10000$," Flow, Turbulence and Combustion **92**, 451–471 (2014).

[19] Mohammad Hossein Shafiei Mayam, *Experimental study of the turbulence structures in a boundary layer subjected to a strong adverse pressure gradient*, Ph.D. thesis, Université Laval (2009).

[20] Per Egil Skare and Per-Åge Krogstad, "A turbulent equilibrium boundary layer near separation," Journal of Fluid Mechanics **272**, 319–348 (1994).

[21] AG Gungor, Y Maciel, MP Simens, and J Soria, "Scaling and statistics of large-defect adverse pressure gradient turbulent boundary layers," International Journal of Heat and Fluid Flow **59**, 109–124 (2016).

[22] Martin Skote and Dan S Henningson, "Direct numerical simulation of a separated turbulent boundary layer," Journal of Fluid Mechanics **471**, 107–136 (2002).

[23] Philippe R Spalart and Jonathan H Watmuff, "Experimental and numerical study of a turbulent boundary layer with pressure gradients," Journal of Fluid Mechanics **249**, 337–371 (1993).

[24] Alexandra Bobke, Ricardo Vinuesa, Ramis Örlü, and Philipp Schlatter, "History effects and near equilibrium in adverse-pressure-gradient turbulent boundary layers," Journal of Fluid Mechanics **820**, 667–692 (2017).

[25] Ricardo Vinuesa, Alexandra Bobke, Ramis Örlü, and Philipp Schlatter, "On determining characteristic length scales in pressure-gradient turbulent boundary layers," Physics of Fluids (1994-present) **28**, 055101 (2016).

[26] Y. Maciel, K. S. Rossignol, and J. Lemay, "A study of a turbulent boundary layer in stalled-airfoil-type flow conditions," Exp. Fluids **41**, 573–590 (2006).